Magnetization reversal and domain correlation for a non-collinear and out-of-plane exchange-coupled system

2011 New J. Phys. 13 063008

(http://iopscience.iop.org/1367-2630/13/6/063008)

New Journal of Physics
The open-access journal for physics

Magnetization reversal and domain correlation for a non-collinear and out-of-plane exchange-coupled system

Amitesh Paul[1,3], N Paul[1] and Stefan Mattauch[2]

[1] Helmholtz-Zentrum Berlin für Materialien und Energie GmbH, Hahn-Meitner-Platz 1, D-14109 Berlin, Germany

[2] Jülich Centre for Neutron Science JCNS, Forschungszentrum Jülich GmbH, Outstation at FRM II, Lichtenbergstraße 1, 85747, Garching, Germany

E-mail: amitesh.paul@helmholtz-berlin.de

New Journal of Physics **13** (2011) 063008 (20pp)
Received 18 January 2011
Published 8 June 2011
Online at http://www.njp.org/
doi:10.1088/1367-2630/13/6/063008

Abstract. We have investigated the impact of *out-of-plane* ferromagnetic (FM) anisotropy (which can be coincident with the direction of unidirectional anisotropy), where antiferromagnetic (AF) anisotropy is along the film plane. This provides a platform for non-collinear exchange coupling in an archetypal exchange coupled system in an *unconventional* way. We probe the in-plane magnetization by the depth-sensitive vector magnetometry technique. The experimental findings reveal a magnetization reversal (i) that is symmetric for both the branches of the hysteresis loop, (ii) that is characterized by vertically *correlated* domains associated with a strong transverse component of magnetization and (iii) that remains untrained (suppression of trained state) with field cycling. This scenario has been compared with in-plane magnetization reversal for a *conventional in-plane* unidirectional anisotropic case in the same system that shows usual asymmetric reversal and training for vertically *uncorrelated* domains. We explain the above observations for the out-of-plane case in terms of inhomogeneous magnetic states due to competing perpendicular anisotropies that result in non-collinear FM–AF coupling. This study provides direct evidence for the vertical correlation of domains mediated by out-of-plane exchange coupling.

[3] Author to whom any correspondence should be addressed.

Contents

1. Introduction

It is well known that the interfacial exchange coupling between a ferromagnet (FM) and an antiferromagnet (AF) can 'lock' the magnetization into the FM in a well-defined direction that makes the system biased. This effect takes the form of a unidirectional magnetic anisotropy and is known as the exchange bias [1]. A cooling field H_{FC} (cooling below the ordering temperature of the AF in a definite direction) essentially determines the state of the FM, which in turn plays a role in determining the strength of the bias field H_{EB} [2, 3]. Apart from the direction, the strength of the cooling field can also be a determining factor if it is below the saturation field of the FM (which in most cases is only a few Oe) [4].

The basic understanding of the origin of the effect has been summarized in recent reviews [5]. Exchange bias is associated with many salient features such as coercivity enhancement [6, 7], asymmetric hysteresis loops [8, 9] and training effect [10]. However, all these features are associated with the conventional unidirectional anisotropy in a system. In the conventional case, the cooling field is applied in the film plane along a certain direction and this direction normally (almost) coincides with the AF anisotropy axis as well. It has been shown earlier, from neutron-scattering experiments, that the magnetization reversal in such systems is dependent on the variation in the different anisotropy energies involved [11].

1.1. In-plane collinear coupling

The strength of the exchange bias is known to be proportional to the projection of the 'frozen-in' AF spins onto the H_{FC} direction, which in most cases is also the FM easy axis. As mentioned above, usually the cooling magnetic field is along the direction of the FM uniaxial anisotropy. In the case where the cooling field is along a direction that is away from the FM uniaxial anisotropy, the FM moments are likely to align along the H_{FC} direction at least for certain materials (provided it is more than the saturation field of the FM). This in turn also aligns the AF

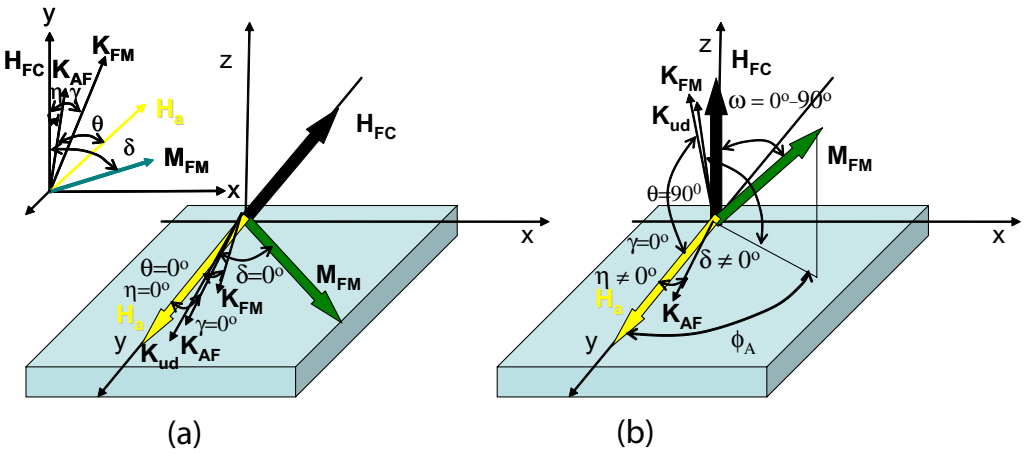

Figure 1. Illustration of the different anisotropy axes for (a) in-plane and (b) out-of-plane cooling geometry.

spins along the same direction (collinear). This is a usual case of collinear coupling where the three anisotropy directions, namely the unidirectional, the uniaxial AF and the FM anisotropy coincide. This has been observed for a conventionally cooled CoO/Co system, for example.

Phenomenologically, the free energy per unit area of the AF–FM bilayer can be written as

$$E = -K_{\mathrm{FM}} t_{\mathrm{FM}} \sin^2(\delta - \gamma) - J_{\mathrm{E}} M_{\mathrm{AF}} M_{\mathrm{FM}} \cos\delta - H_{\mathrm{a}} M_{\mathrm{FM}} \cos(\delta - \theta) t_{\mathrm{FM}}, \qquad (1)$$

where the first term represents the *uniaxial* anisotropy energy of the FM layer with the anisotropy constant K_{FM}. The second term is the *unidirectional* anisotropy energy characterized by the exchange coupling constant J_{E}. The unidirectional anisotropy K_{ud} is embedded in $J_{\mathrm{E}} M_{\mathrm{AF}} M_{\mathrm{FM}}$ as the exchange field is expressed as $H_{\mathrm{ex}} = J_{\mathrm{E}} M_{\mathrm{AF}}$. Finally, the last term stands for the Zeeman energy for a field H_{a}. Here δ is the angle between M_{FM} and the easy axis, γ is the angle between K_{FM} and H_{ex}, whereas θ is the angle between H_{a} and the AF anisotropy axis or the H_{FC} direction, where M_{FM} and M_{AF} are the respective magnetizations. In the case of conventional in-plane field cooling, γ is zero (the field cooling axis coincides with the anisotropy axis), θ is generally $\sim 0/180^\circ$ as H_{a} is applied along the H_{FC} direction. Thus for $\delta \approx 0^\circ$, one can observe non-uniform magnetization reversal since the angle between the effective field (resultant of the three anisotropy fields along their respective directions) and the M_{FM} direction is small [11]. A schematic representation of different anisotropy axes corresponding to the in-plane cooling field is shown in figure 1(a).

1.2. In-plane non-collinear coupling

Apart from the conventional case discussed above, there have been reports of a possibility that the easy axis of the FM and that of the AF are not parallel, i.e. they may remain *non-collinear*. In the event that the orientation of the FM is not properly maintained with respect to the AF (owing to an insufficient field or temperature, or sometimes intrinsic), one may end up with a non-collinear arrangement in the system [12]. Typical examples of intrinsic in-plane non-collinearity can be found in epitaxial FeF_2 (twin-axis) systems with off-axis AF and FM spin orientations [13]. Along a collinear anisotropy axis, the exchange bias would be maximum,

whereas along a perpendicular orientation of the anisotropy axis, the exchange bias would be zero. Gräet *et al* [14] used the ferromagnetic resonance technique to determine the *in-plane* misalignment between the FM and AF anisotropy axes in a NiO-based system, which was due to structural disorder. They found that such a misalignment produces asymmetry in the azimuthal behavior of the resonance field, i.e. different angles of the AF and FM anisotropy axes with respect to the applied field axis. The temperature dependence of non-collinearity between in-plane unidirectional anisotropy and FM layer uniaxial anisotropy was addressed in a CoO/Co system [15]. For a zero-field cooled configuration, M_{FM} was found to deviate from its frozen-in direction toward the FM uniaxial direction with an increase in temperature. Recently, we have also reported a signature of a similar deviation in local anisotropy direction from the unidirectional one, for remanent field cooled state in CoO/Co, leading to uniform magnetization reversal [10].

1.3. Out-of-plane coupling

Along with in-plane biased systems, there have been some interesting studies on *out-of-plane* bias (perpendicular) systems as well. Generally, these include systems designed for strong perpendicular anisotropies (out-of-plane magnetic easy axis and in-plane hard axis, e.g. Co/Pt multilayers exchange biased with CoO) [16]. However, the magnetization reversal mode was observed only via coherent rotation (uniform reversal mode) for the out-of-plane loop (similar to that observed for in-plane loops) rather than via domain wall motion and nucleation (non-uniform mode). Ijiri *et al* [17], on the other hand, reported 90° orientation (coupling) between the Fe_3O_4 and the in-plane epitaxial CoO spins as a consequence of the interfacial exchange coupling giving rise to exchange biasing in a complicated anisotropic system (multiple symmetrical axis). Recently, different field cooling options were explored in IrMn (Co/Pt-based) systems [18]. The samples that were field cooled out-of-plane and measured in-plane showed no bias field, indicating that the uncompensated AF spins remained orthogonal to the FM spins. In another case, a Ni layer was saturated by an out-of-plane field perpendicular to the FeMn wedge [19]. This caused the FeMn ions to tilt toward the vertical direction. Recently, perpendicular anisotropy in exchange biased Co–Pt has been shown to be dependent on the ordering temperature of CoO [20].

1.4. Unconventional coupling

Usually (conventionally), the magnetization is probed along the plane of the exchange biased direction. The exchange bias direction (unidirectional anisotropy) can be in plane or out of plane, as the AF anisotropy can also lie along or in the plane of the exchange anisotropy. In such cases, magnetization perpendicular to the exchange anisotropy direction typically shows a hard-axis-type behavior.

One must remember that in the case of polycrystalline layers, one can assume randomly oriented grains (e.g. CoO) with uniaxial anisotropy. Without a cooling field they can be treated as a spin-glass-type system [10]. Here the local magnetization is randomly oriented along the anisotropy axis. The local anisotropy axis is then predominantly directed along the direction of remanent magnetization. On the other hand, the application of a sufficiently strong external field can lead to a macroscopic net magnetization originating from the exchange interaction between uncompensated spins [23]. In such a case, the local anisotropy axis is obviously oriented along

the cooling field direction. This is not surprising because the easy axis results from the averaging over the grains within the volume of the exchange length. In the case of out-of-plane field cooling, this local anisotropy axis can therefore be out of plane. A schematic representation of different anisotropy axes corresponding to the out-of-plane cooling field is shown in figure 1(b).

The realization of perpendicular exchange bias and perpendicular anisotropic magnetic nano-structures has great implications for ultrahigh density perpendicular recording media development [21, 22]. The aim of this work is to explore the option of realizing out-of-plane exchange coupling (unconventional) in a system with in-plane anisotropy. In this study, we particularly address the issue of magnetization reversal in an exchange biased system where the AF anisotropy is oriented perpendicular to the out-of-plane unidirectional anisotropy. We show that, in this way, one can effectively modify the magnetic correlation of domains (in-plane and out-of-plane) which were otherwise uncorrelated.

In our CoO/Co system, the uncompensated AF spins are frozen-in by the exchange field of the FM moments as a large enough field aligns the FM moments (almost saturates the FM moments out of plane [21]) along a direction perpendicular to the film plane. This establishes or induces the exchange bias direction. The AF spins, on the other hand, deviate from the initial cooling field direction toward their closest in-plane easy axis (cubic anisotropy) once AF order sets in and remain so also during measurements along an in-plane direction [12]. They are restricted to the film plane (which may not coincide with the applied field direction) for our polycrystalline Co films with a controlled film thickness of 5.0 nm. An out-of-plane AF easy axis can be ruled out due to strong in-plane interfacial anisotropy, which can be exhibited only below 1.0 nm. Co is known to have a strong uniaxial magnetocrystalline anisotropy of 6.5×10^6 (4.5×10^6) erg cc^{-1} at 10 K (300 K) [24]. The unidirectional anisotropy axis, on the other hand, at the field-cooled temperature, would remain out of plane. This would intrinsically provide the primary platform for non-collinear coupling. Since the applied field lies in the film plane, the magnetization reversal for such a system would be dependent on the effective field due to the vector sum of the applied field and the three anisotropy fields corresponding to the energies K_{ud}, K_{AF} (making angles θ and η with H_a, respectively) and K_{FM} (making an angle δ with the in-plane projection of M_{FM}). Here γ can be considered as 0° in the case that the FM axis coincides with the field cooling axis.

The FM spins are expected to exchange couple the out-of-plane uncompensated AF spins either by turning completely ($\omega = 0^\circ$) to align with the uncompensated AF spins (which would render a collinear coupling) or by making a finite angle ($0^\circ < \omega \leqslant 90^\circ$) between them (which would render a non-collinear coupling). If the FM spins are completely re-oriented out of plane (plausibly during field cooling), then one would only observe typical hard-axis-type behavior (via uniform mode) while measuring its magnetization along the film plane [18]. This is because of the large effective angle [11] that would result due to large θ ($\approx 90^\circ$) and the small in-plane exchange field component that may not result in any in-plane bias field [18]. On the other hand, if the FM spins make an angle, then a considerable component of the FM magnetization would lie in the film plane. Now if one measures along the film plane, only then can one have a chance to observe a signature of non-collinear coupling for which the magnetization reversal can be via non-uniform mode as well. This is because, in spite of a large θ, the effective angle that would be realized can be small enough owing to a large in-plane exchange field component.

We present here a depth-sensitive investigation of magnetization reversal for an archetypal exchange coupled system (CoO/Co). For a comparative measurement between an conventional and a unconventional case, two different unidirectional anisotropy directions were induced on

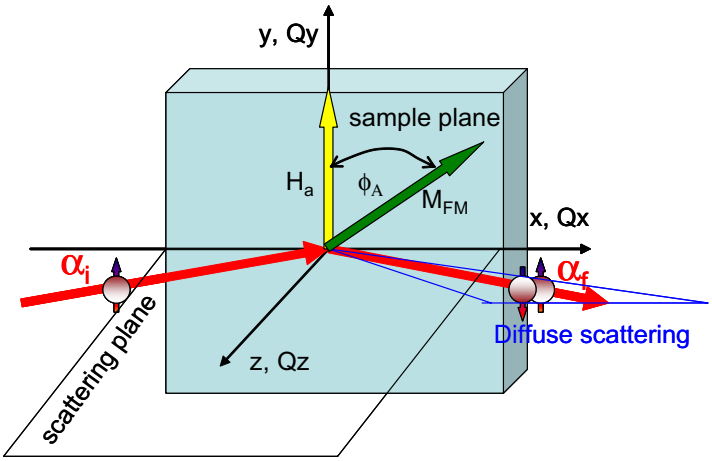

Figure 2. Schematic representation of scattering geometry for a polarized neutron.

applying (i) a cooling field ($H_{FC} = +4.0\,\text{kOe}$) directed along the out-of-plane direction of the system (unconventional) and (ii) a cooling field ($H_{FC} = +4.0\,\text{kOe}$) directed along an in-plane direction (conventional). We have used the same sample after heating it up to room temperature (RT) before cooling it again. We show that the in-plane magnetization reversal mechanism is clearly different for the above two cases. A completely new spin distribution can be envisaged for our unconventional exchange coupled system.

1.5. Neutron scattering measurements

We have used depth-sensitive neutron scattering under grazing incidence with polarization analysis (PNR) for the identification of reversal mechanisms in exchange bias systems [3, 8, 9]. Owing to the interaction between polarized neutrons and magnetic moments in the specimen, PNR is sensitive to the in-plane magnetization for a homogeneous film on a *microscopic* scale. Neutron scattering with polarization analysis can discriminate between the longitudinal and transverse components of magnetization.

The neutron interaction potential is given by

$$V = \frac{2\pi\hbar^2}{m}(\rho_n \pm \rho_m) = \frac{2\pi\hbar^2}{m} N\, b_n + \mu_N \vec{\sigma} \cdot \vec{B}, \tag{2}$$

where N $(= \text{density} \times N_A \times M^{-1}\,\text{cm}^{-3})$ is the number density, b_n the coherent nuclear scattering length, m the neutron mass, M the atomic mass (g mol^{-1}) and B the internal magnetic field of the specimen; $\vec{\sigma}$ represents the operator associated with the Pauli spin matrices, whereas μ_N is the nuclear magneton. The neutron magnetic moment is expressed as $\mu_N = -g_n \mu_N S_n$, where S_n $(=\vec{\sigma}/2)$ is the spin-1/2 operator and g_n is the g-factor of the nucleon related to the gyromagnetic ratio γ_N $(= 1.913)$. The scattering-length densities (SLD) of a magnetic specimen are given by either the sum or difference of the nuclear (ρ_n) and magnetic (ρ_m) components. The $\pm$ signs refer to the spin-up and spin-down states of the incident neutron with respect to the polarization of the specimen.

A detailed description of the technique and measurements can be found in ([25], see also [28]). A schematic representation of the scattering geometry is given in figure 2. Within the framework of specular scattering geometry, one probes the normal wave vector transfers

$q_\perp = \frac{2\pi}{\lambda}[\sin(\alpha_i) + \sin(\alpha_f)]$. Off-specular scattering contributions along the in-plane momentum transfer vector $q_\parallel = \frac{2\pi}{\lambda}[\cos(\alpha_f) - \cos(\alpha_i)]$ arise when the in-plane translational symmetry is broken by interface waviness (roughness) or by magnetic domains on a length scale shorter than the neutron coherence length ($l_\parallel$) along $q_\parallel$. The non-spin flip (NSF) scattering amplitude provides information on $\rho_n \pm \rho_m \cos\phi_A$, and the spin flip (SF) channels measure $\rho_m^2 \sin^2\phi_A$ if the domain size is larger than the projection of the neutron coherence length along the sample plane ($l_\parallel$). Here ϕ_A is the angle between the magnetization M and the applied field H_a (which can also be the neutron quantization axis). In the experiment, four different cross sections can be distinguished: NSF (R_{++} and R_{--}) and SF (R_{+-} and R_{-+}) channels. Here + and − signs are used to distinguish the intensity contributions R representing a polarization component ∥ or anti-∥ to the guiding field, respectively. $R_{++/--}$ contains the sum/difference between the nuclear (ρ_n) and magnetic scattering (ρ_m), whereas the SF signal contains only the magnetic information.

One may note that the illuminated part of the sample surface is usually much larger than the projection of the coherence volume of the neutron beam. The scattered intensity that one measures is, in the case of specular scattering, the depth variation of laterally averaged interaction potential from different coherent volumes (defined by $Q_\parallel = 0$ as the surface is considered homogeneous and flat). Mean magnetization, averaged over the coherence volume, is responsible for the specular reflection. For domains larger than $Q_\parallel$, the intensities reflected from different domains superimpose incoherently in the specular beam [26–28].

The unit vector of $\vec{B}$ defines the quantization axis of the neutron spin. The two eigenvectors $|+\rangle$ and $|-\rangle$ of the operator $\vec{\sigma}\cdot\vec{B}$ determine the spin projection along the quantization axis. A linear combination of these two eigenstates essentially provides the solution to the Schrödinger equation for an incoming plane wave vector ($\vec{k}_i$) with in-plane component $\vec{\kappa}_i$. Now, taking into account the continuity relations at the interfaces and its first derivative, one can solve the Schrödinger equation for each layer following the recursion formula of Parratt to deduce the reflectivity [29].

We employ distorted wave Born approximation (DWBA) to simulate the off-specular scattering ([25], see also [28]). In our model, the mean magnetization w.r.t. the applied field varies from region to region around a mean angle ϕ_A with a Gaussian distribution of width $\Delta\phi_A$. In this model, both the components of magnetization parallel (along the y-axis) and perpendicular (along the x-axis) to H_a will contribute to the diffuse scattering signal.

As long as the condition of translational invariance holds (within a certain coherent volume) it will not lead to any off-specular scattering. Thus, the scattered intensity that one measures is, in the case of specular scattering, the depth variation of laterally averaged interaction potential from different coherent volumes (defined by $Q_\parallel = 0$). However, when the invariance is broken (but on a length scale smaller than $l_\parallel$), off-specular scattering may be seen, which measures the fluctuations around the mean value of the laterally averaged interaction potential. The fluctuations are given by the dispersion along the longitudinal and transverse directions

$$\Delta\phi_A(L)^2 = \langle\cos^2\phi_{A'}\rangle_{coh} - \langle\cos\phi_{A'}\rangle_{coh}^2 \tag{3}$$

or

$$\Delta\phi_A(T)^2 = \langle\sin^2\phi_{A'}\rangle_{coh} - \langle\sin\phi_{A'}\rangle_{coh}^2.$$

Due to the influence of dynamical effects (multiple scattering due to refraction and total external reflection) close to the critical angle of total reflection, DWBA is used instead of Born

approximation. In this approach, the potential operator in each layer can be decomposed into a sum of the reference potential and perturbation contribution in the form

$$V(x, y, z) = \langle V \rangle(z) + V_{\text{perturbed}}(x, y), \tag{4}$$

where $\langle V \rangle(z)$ denotes the reference potential averaged over all lateral coordinates (x, y), which is responsible for specular scattering, while $V_{\text{perturbed}}(x, y)$ causes the off-specular scattering signatures. The z-axis dependence is taken care of by the propagation operator $\widehat{S}(z)$ inside each layer n. The perturbed potential includes the nuclear and magnetic scattering length density fluctuations. Off-specular scattering affected by dynamical effects (close to the critical angle of total reflection) can be taken into account within the reflection and transmission coefficients involved.

We may restrict the fluctuations (which may have their origins in the magnetic fields at the interface and/or within the layers) as arising only from bulk density fluctuations separated by smooth interfaces (as in the cases of magnetic domains). This eventually simplifies the equations involved without affecting the physics in general. Now, $V_{\text{perturbed}}(x, y)$ can be written as

$$V_{\text{perturbed}}(x, y) = \frac{2\pi\hbar^2}{m}(\rho_{n'} \pm \rho_{m'}), \tag{5}$$

where $\rho_{n'}$ and $\rho_{m'}$ denote the respective lateral scattering length density fluctuations. Thus the scattering amplitude $F(\vec{k}_{\text{f}}, \vec{k}_{\text{i}})$ takes the form

$$F(\vec{k}_{\text{f}}, \vec{k}_{\text{i}}) = -\frac{m}{2\pi\hbar^2}\Sigma n \int \langle \psi_{fn}(\vec{k}_{\text{f}}, r) \mid V_{\text{perturbed}} \mid \psi_{\text{in}}(\vec{k}_{\text{i}}, r) \rangle \mathrm{d}r, \tag{6}$$

where $\vec{k}_{\text{i}}$ and $\vec{k}_{\text{f}}$ denote the incident and final wave vectors and the integration is over the coherence volume intersection, which is summed over the volume n. Note that the perturbed potential is taken between the bra and the ket instead of the reference potential as in the case of Born approximation.

Owing to different asymptotic conditions (both the incident and the final wave assume the plane wave to be emanating from the sample and approaching the sample from the detector as well as from the source, i.e. the reference potential is not dependent on the lateral coordinates), the scattering amplitude takes the form

$$F(\vec{k}_{\text{f}}, \vec{k}_{\text{i}}) = -\frac{m}{2\pi\hbar^2}\langle \psi_{f0}(\vec{k}_{\text{f}}, 0) \mid \upsilon_{fi} \mid \psi_{i0}(\vec{k}_{\text{i}}, 0) \rangle, \tag{7}$$

where υ_{fi} includes the summation over n, the integral involving the respective incident and final propagators $\widehat{S}(z)$ in n and the lateral Fourier transform of the perturbed potential $F(Q_{\parallel})$ in the layer

$$F(\vec{k}_{\text{f}}, \vec{k}_{\text{i}}) = \Sigma_l \int \widehat{S}_f(z) \cdot F(Q_{\parallel}) \cdot \widehat{S}_i(z) \mathrm{d}z, \tag{8}$$

where

$$F(Q_{\parallel}) = -\frac{2\pi\hbar^2}{m} \int \mathrm{e}^{-\mathrm{i}Q_{\parallel}\cdot(x,y)} V_{\text{perturbed}}(x, y)\, \mathrm{d}(x, y). \tag{9}$$

Further, by decomposing it into linear combinations of the Pauli spin matrices and unit matrices (embedded within the reflection and transmission amplitude operators), the lateral Fourier transform of the perturbed potential can be written as the Fourier transform of the pair correlation functions involving nuclear and magnetic fluctuations.

The Fourier transform of the pair correlation functions for transverse as well as longitudinal fluctuations (averaging over the surface of the coherence regime and integrating along the unresolved y-axis) within a laterally homogeneous length scale of $2\xi(x, y)$ can be expressed as functions of Lorentzian shapes

$$\langle F(Q_{x,y}) \cdot F^*(Q_{x',y'})\rangle \approx \mathcal{C}(xx', yy') \cdot \left[\frac{\xi(x, y)}{1+(Q\cdot\xi(x, y))^2} + \frac{\xi(x', y')}{1+(Q\cdot\xi(x', y'))^2}\right], \tag{10}$$

where $\mathcal{C}(xx', yy')$ are the respective amplitudes of fluctuations parallel and perpendicular to the quantization axis.

1.6. Samples and measurements

We have investigated a multilayer of the composition $SiO_2/[Co(11.0\,nm)/CoO(5.0\,nm)/Au(22.5\,nm)]_{16}$ with different sequential field cycles. Details of similar sample growth procedures have been published earlier [30]. Essentially, we employed an ultraviolet light-assisted oxidation at an O_2 pressure of 200 mbar at 50 °C for 1 h. Conventional in-plane magnetization loops were measured using a superconducting quantum interference device (SQUID) MPMS from Quantum Design. For magnetic studies, the samples were typically cut into mm^2 pieces, and both in- and out-of-plane orientations were probed. For all out-of-plane measurements the sample pieces were cut to a size that could be clamped inside the straw without any further means of holding the sample in place. Since the net magnetic moment is small for out-of-plane measurements, the signal-to-noise ratio is small. The data obtained include the temperature-independent paramagnetic-like response, but exclude the diamagnetic response (from the sample-holder and the clean substrate with dimensions similar to that of the investigated sample) [31].

Granular structure of the film was confirmed from the height–height correlation function using atomic force microscopy (AFM) measurements. The AFM measurements were carried out in tapping mode using a multimode scanning probe micrometer from Digital Instruments. The grain structure of the film was also observed utilizing scanning electron microscopy (SEM). Microstructural characterization has been done using cross-sectional transmission electron microscopy (XTEM).

The neutron scattering experiments were performed at the polarized neutron reflectometer with polarization analysis TREFF at the FRM-II for a wavelength of 4.73 Å, measuring the specular and off-specular data simultaneously. All measurements have been made after the sample was cooled to 10 K from RT by a continuous-flow cryostat in the presence of a defined cooling field provided by an electromagnet. The neutron measurements were made with magnetic field in the sample plane, which is $\perp^r$ / $\parallel$ to the initial cooling field direction. Since neutron scattering signal is insensitive to the magnetization component parallel to the scattering vector (surface normal), in the case of non-collinear coupling, the magnetization can be measured along a direction different from the FM easy axis.

Alignment of the perpendicular field axis to that of the sample plane was particularly taken care of by using a laser on top of the sample surface. The laser gets reflected from the sample plane and the reflected spot was matched with the laser source spot within a high level of precision. The direction of the field was flipped (turning the magnet) with respect to the sample plane during the course of the experiment so as to access the fields along two different branches (decreasing and increasing) of the hysteresis loop residing on the positive and negative axes, respectively. This is particularly necessary for neutron measurements at a

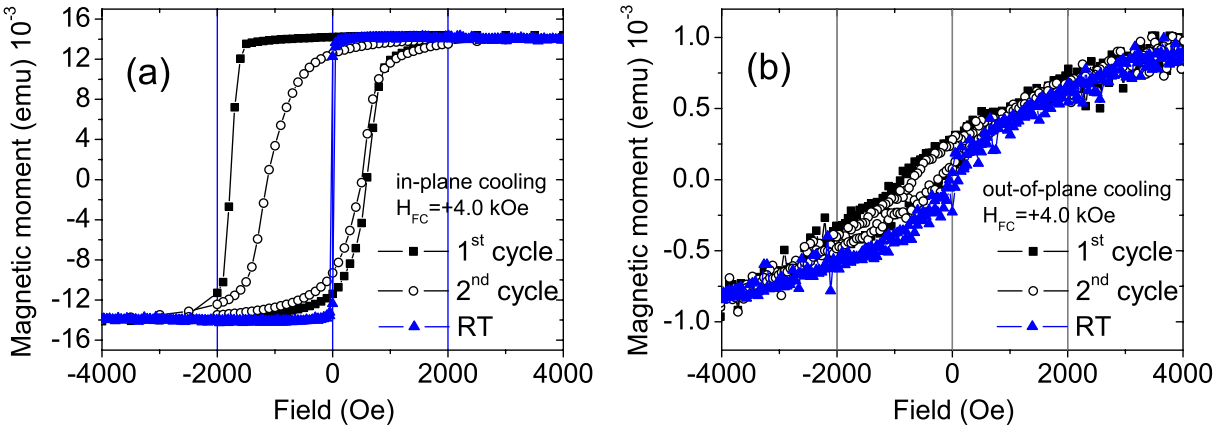

Figure 3. SQUID magnetization for the CoO/Co/Au ML for (a) a conventional in-plane cooling field and (b) a non-conventional out-of-plane cooling field.

reflectometer beamline as the measurements can only be possible with a constant direction of field (as that of the guiding field) maintaining the polarization of the neutron beam. Such an arrangement obviously confirms a perfect perpendicular alignment of our cooling field with respect to the sample plane as we compare the results from the decreasing and increasing branches of the hysteresis loop. These situations are compared with the conventional case where the measurements are made in the sample plane, ||/anti-|| to the cooling field direction.

2. Results and discussion

2.1. Magnetization

We present in figure 3(a) the hysteresis loops for an in-plane cooling field representing the conventional case of in-plane longitudinal (along the applied magnetic field) magnetization measurements. One can see the usual asymmetry in magnetization reversal and disappearance of that asymmetry in reversal just after the first field cycle. The in-plane RT data are also shown. The RT saturation field is around 100 Oe and the coercive field is around 20 Oe for our Co layer. The exchange bias field is ≈ -600 Oe at 10 K. Similar longitudinal magnetization measurements (along the out-of-plane applied magnetic field direction) for out-of-plane cooling are presented in figure 3(b) as we measure along the cooling field axis or in the direction perpendicular to the film plane. The corresponding RT data show that the perpendicular field of 4.0 kOe is not sufficient to completely saturate our specimen out-of-plane (a reduction in net magnetic moment is obviously due to a much smaller size/volume of the sample). However, the loop shift indicates that the system must have been very close to the saturation (single domain) state. In case of a multi-domain state (at a remanence field), the lateral shift in the loop would have been minimal. With an increase in the strength of the perpendicular cooling field (e.g. +8.0 kOe) we could find an increase in the lateral shift or the exchange bias field. Unlike the in-plane case, the loops corresponding to the first and second field cycles are similar for perpendicular field cooling (yet not overlapping). This indicates a similar symmetric magnetization reversal mechanism. The exchange bias field along the cooling field axis for such an out-of-field cooling is estimated to be around -500 Oe in comparison to -600 Oe for the

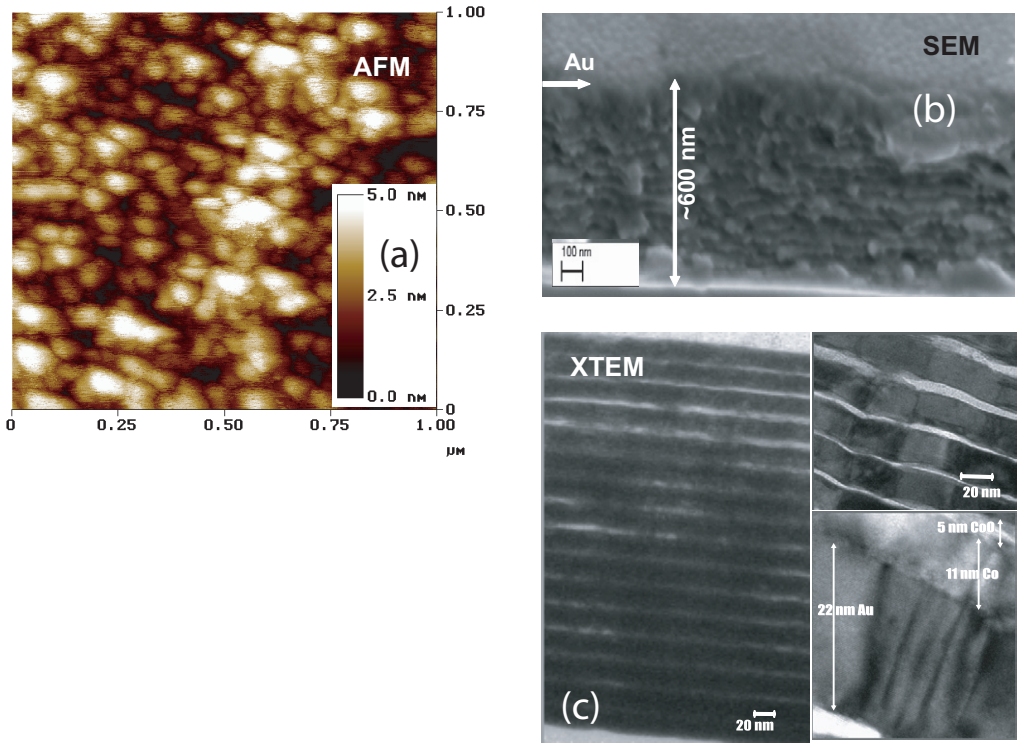

Figure 4. (a) AFM micrograph ($1 \times 1\ \mu m^2$) for a CoO/Co film before depositing the Au layer. (b) Cross-sectional SEM image of the ≈ 616 nm multilayer. (c) Cross-sectional TEM images are shown for the 16-layered structure with sharp interfaces. The lower inset shows the nanostructures of a single layer with vertical correlation of grains.

in-plane cooling field. This obviously indicates that the FM anisotropy axis lies along the cooling field axis; otherwise one would have observed a typical hard-axis-type loop without a loop shift.

2.2. Microstructure

In figure 4(a), we show the granular structure of the CoO/Co film (before depositing the last Au layer on top) using AFM. The average grain size (topmost layer) is estimated to be around 50.0 nm. Figure 4(b) shows SEM images of the cross-section (corrugations are due to the mechanically cleaved sample) of the complete 16-layered structure of Co/CoO/Au ML. The thicknesses of the individual layers are in agreement with the nominal thickness. The morphology of the top Au layer can be estimated to be around 50.0 nm (similar to that of the Co layer grains). All grains are practically of the same size and are distributed homogeneously on the surface. Transmission electron microscopy studies have been carried out on cross-sectional samples prepared by standard mechanical (diamond) polishing followed by Ar^+ ion milling at 4 kV for about 1 h. The conventional bright-field imaging mode was used. Figure 4(c) shows 16 repetitions of a three-layered structure with sharp interfaces. The magnification of a trilayer interface in the stack shows the existence of columnar grains ($\approx$ 15–20 nm) that are vertically correlated from layer to layer. The Au layer is ≈ 22.0 nm thick. This Au thickness is sufficiently thick to assume that this can be regarded as 16 independent CoO/Co samples. One can see

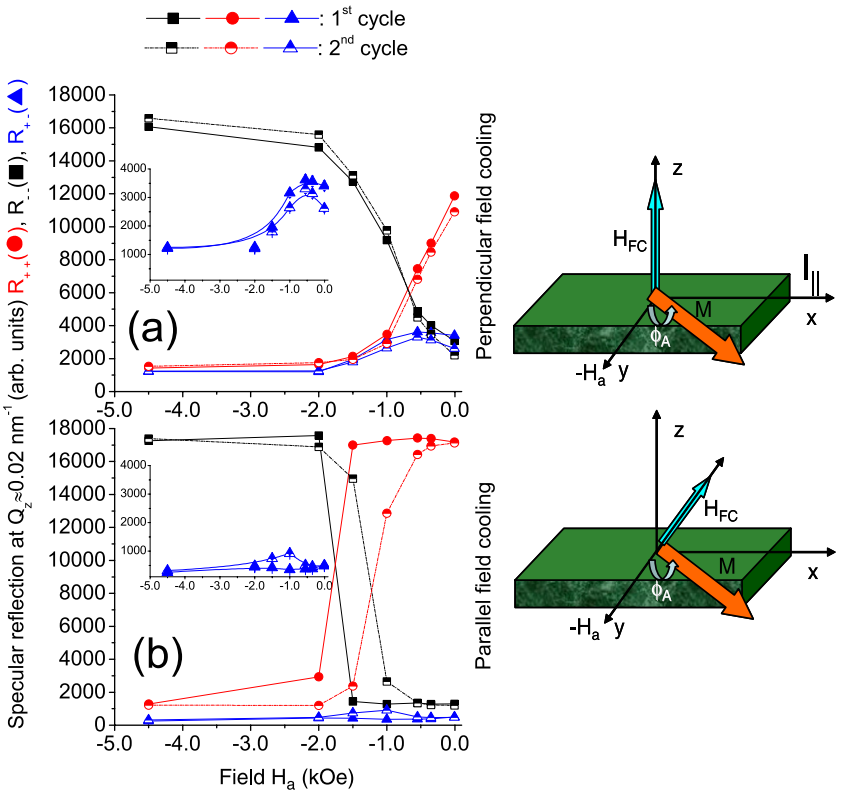

Figure 5. The polarized neutron scattered intensity at $Q = 0.02\,\text{Å}^{-1}$ is plotted against field during various field cycles: the first half of the first field cycle and the first half of the second field cycle after (a) out-of-plane ($\perp^r$) cooling and (b) in-plane ($\parallel$) field cooling. The lines in the panels are a guide to the eye. The insets show the respective SF intensities on a lower scale.

that the vertical correlation of Au layers is not propagating through the CoO layers and would thereby only add the neutron scattering signal from multiple similar interfaces.

2.3. Vector magnetometry

In figure 5, we show the polarized specular reflectivity at a fixed $Q_\perp = 0.02\,\text{Å}^{-1}$ value (corresponding to the highest intensity) for the variation of applied field values (a) $\perp^r$ to the cooling field direction and (b) $\parallel$ to the cooling field direction for the first half of the first field cycle and the first half of the second field cycle, respectively. Measurements are along the *decreasing* branch of the hysteresis loop [3] (sign of H_{FC} opposite to that of H_{a}). The two coercive fields for the out-of-plane cooling field are $H_{\text{C1}} = H_{\text{C1}'} = -650\,\text{Oe}$ and that for the in-plane cooling field are $H_{\text{C1}} = -1760\,\text{Oe}$ and $H_{\text{C1}'} = -1150\,\text{Oe}$. These are the respective reversal points where the R_{++} and R_{--} cross each other. The coercive field values for in-plane field cooling are in agreement with our SQUID measurements. The corresponding SF channel intensities are also plotted (R_{+-} and R_{-+}). In the case of perpendicular field cooling, the coercive field for the *increasing* branch (sign of H_{FC} similar to that of H_{a}) is around 300 Oe, which estimates the in-plane exchange bias field to be around $-175\,\text{Oe}$. This is not equivalent to measuring the transverse component of the magnetization in SQUID after perpendicular field cooling, as the applied field here is in plane. This situation could not be replicated in SQUID.

For parallel field cooling, the lack of high enough SF intensities (during the first half of the first field cycle) and an increase in intensity (during the first half of the second field cycle) can be easily correlated with the typical respective signatures of non-uniform and uniform modes of reversal [11]. On the other hand, for $\perp$ field cooling, a significant increase in the SF signal signifies a magnetization reversal that is predominantly via coherent rotation (stronger transverse component). Furthermore, these SF intensities are similar for the respective field cycles. One may also note that an almost overlapping intensity (R_{++}, R_{--} and R_{+-}) variation for the first and the second field cycles already points to the fact that there has been no training effect during the reversal. To check on this further, we inspect the specular reflectivity patterns of the specimen.

The specular reflectivity patterns of the specimen (closed symbols) are plotted together with their least-square fits (open circle) in figures 6(a)–(c) for the $\perp$ field cooling case. We first show the behavior along the decreasing branch of the hysteresis loop. The data show six peaks of the ML in the NSF channels, which are the respective order of Bragg reflections of the ML. In both cases, R_{--} dominates over R_{++} and is related to a net magnetization, collinear to H_a. The fits reveal that the variation in ϕ_A is around 120° (at remanence) and goes to 15° at −4.5 kOe (even at −4.5 kOe, the magnetic moments are very close to an alignment with H_a as compared to complete alignment in the conventional case, indicating an increase in interfacial exchange energy as compared to the conventional case). This uniform (predominantly coherent rotation) angular variation with applied field is very similar for the two field cycles. This similarity clearly points to the fact that there has been a suppression of training. One may note that the respective layer thicknesses are similar to their nominal thicknesses and their magnetic profiles (all determined from that at maximum applied field after parallel field cooling) do not vary with field cycling. The only parameter that was varied with field is ϕ_A. Intensities along the specular line, for conventional parallel field cooling field, are also shown for comparison in figures 6(d) and (e). The specular patterns for the increasing branch of the hysteresis loop (for perpendicular field cooling) are shown in figures 6(f)–(h) (this was done by turning the magnet w.r.t. the sample, thereby effectively cooling the sample at −4.5 kOe instead of +4.5 kOe and in this way the sign of the applied field also remains unchanged). Here, the magnetization reversal takes place also via the uniform way. Thus one can conclude the reversal mechanism is symmetric for both branches of the hysteresis loop. Figures 6(i)–(k) show the reflectivity patterns for the second field cycle along the decreasing branch. Further we show the magnetization angle ϕ_A for the increasing and decreasing branches of the hysteresis loop in figure 6(l).

2.4. Domain correlations

Next, we show the corresponding intensity maps (off-specular and specular SF scattering signals) in figures 7(a)–(f). The intensity along the diagonal $\alpha_i = \alpha_f$ is the specular reflection along $Q_\perp$. These maps are also simulated within the DWBA ([25], see also [28]). The simulations are done by taking into account the various optical effects such as reflection and refraction components (spin-up and spin-down) and convoluting with instrumental resolution. The lateral intensities are due to the perturbation considered. The value of ϕ_A is taken from the fitted values of the specular patterns. We consider the magnetization to fluctuate from domain to domain around the mean angle ($\Delta\phi_A = 30°$) for parallel field cooling. No such fluctuations were considered for perpendicular field cooling, which supports their vertical correlation.

The most interesting feature is perhaps the fact that there has been a vertical correlation of FM domains (lateral sizes are $\approx 10\,\mu$m at remanence and around the reversal point) plausibly

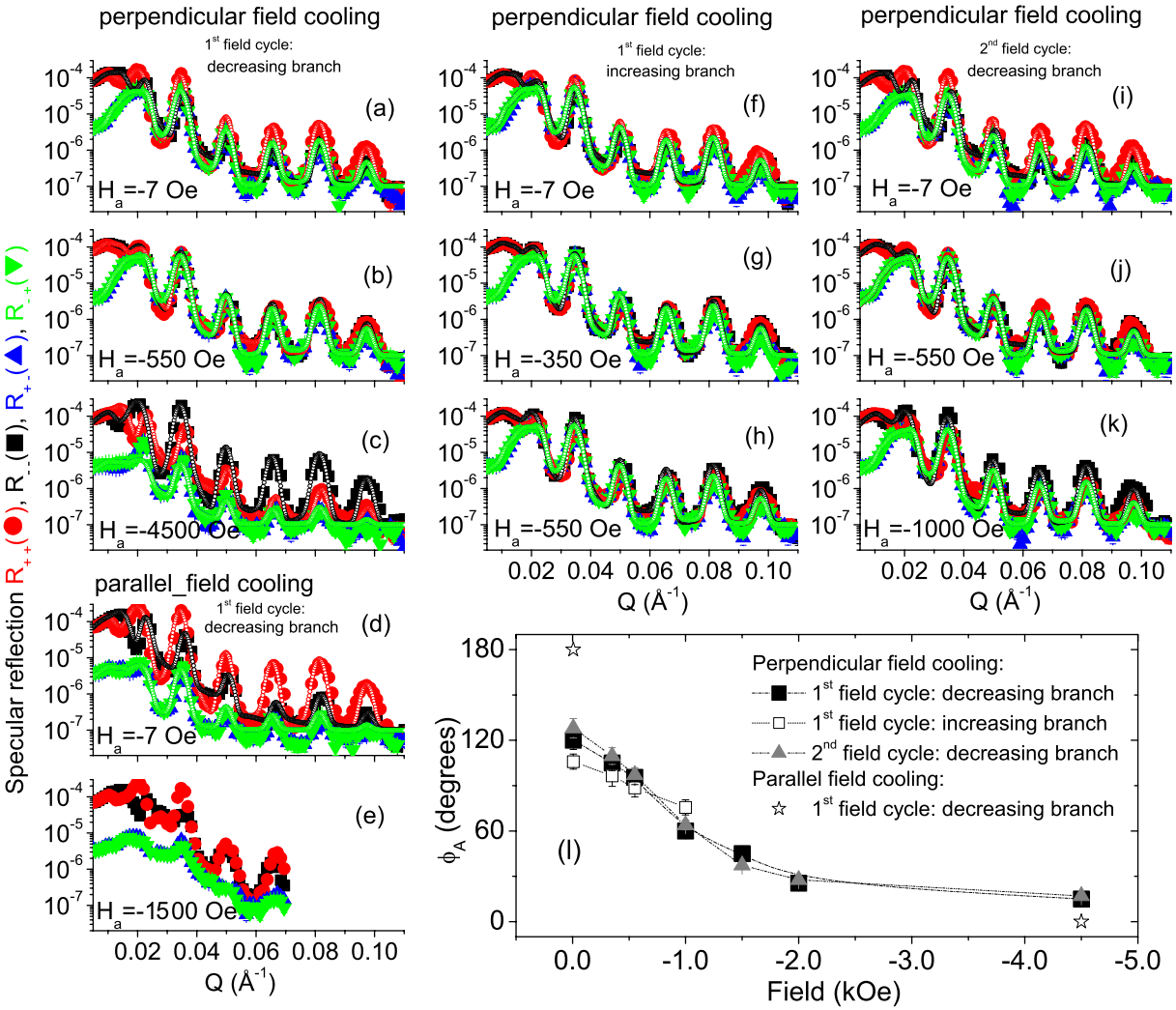

Figure 6. Specular reflectivity patterns (solid symbols) along with their fits (open symbols) for the NSF [R_{++} (red) and R_{--} (black)] and SF [R_{-+} (green) and R_{+-} (blue)] channels measured from Co/CoO/Au ML in different conditions as indicated: (a–c) after *positive* field cooling *perpendicular* to the film plane; (d, e) after *positive* field cooling *parallel* to film plane; (f–h) after *negative* field cooling *perpendicular* to the film plane and measuring along the second half of the first field cycle; and (i–k) after *positive* field cooling *perpendicular* to film plane and measuring for the second field cycle. Solid symbols are the data, and open circles are fits to a model (no fits to the data are shown for parallel field cooling at 1.0 kOe since the intensities are mostly diffusive in nature owing to nonuniform reversal). (l) The respective variation of ϕ_A with H_a. The symbol sizes are representative of the error bars in the measurements.

induced by the perpendicular field cooling. Typical signatures of vertically correlated domains can be seen, as diffuse streaks along $Q_\parallel$ at the position of the Bragg peaks are visible in figures 7(a, b, d, e, g, h). One may note that these diffuse streaks in the SF channels do disappear (figure 7(c, f) at higher fields (−4.0 kOe). This clearly indicates that they are exclusively of magnetic origin and thus establish the *magnetic correlation*. It may be noted that the vertical

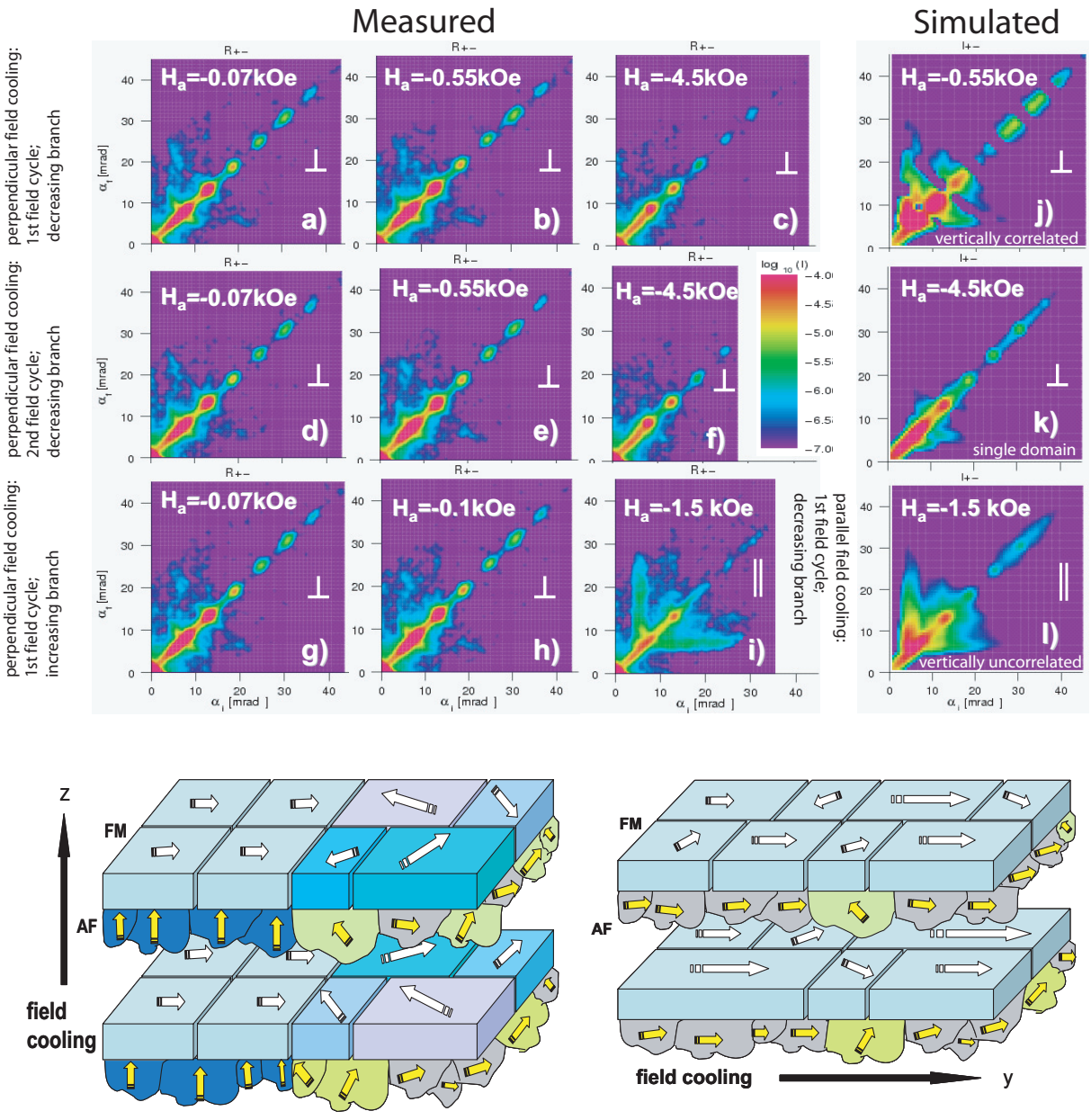

Figure 7. SF intensity maps [R_{-+}] from Co/CoO/Au ML measured at (a–c) perpendicular ($\perp$) field cooling and measured along the first half of the first field cycle, (d–f) the first half of the second field cycle, (g, h) the second half of the first field cycle and (i) parallel ($\parallel$) field cooling along the first half of the first field cycle. The corresponding simulated intensity maps are shown alongside: (j, k) for $\perp$ cooling and (l) for $\parallel$ field cooling. The color bar encodes the scattered intensity on a logarithmic scale. A schematic representation of the AF–FM magnetization corresponding to out-of-plane field cooling (unconventional) and in-plane field cooling (conventional) is shown below. The FM moments are the in-plane projection, whereas the AF moments are the uncompensated ones.

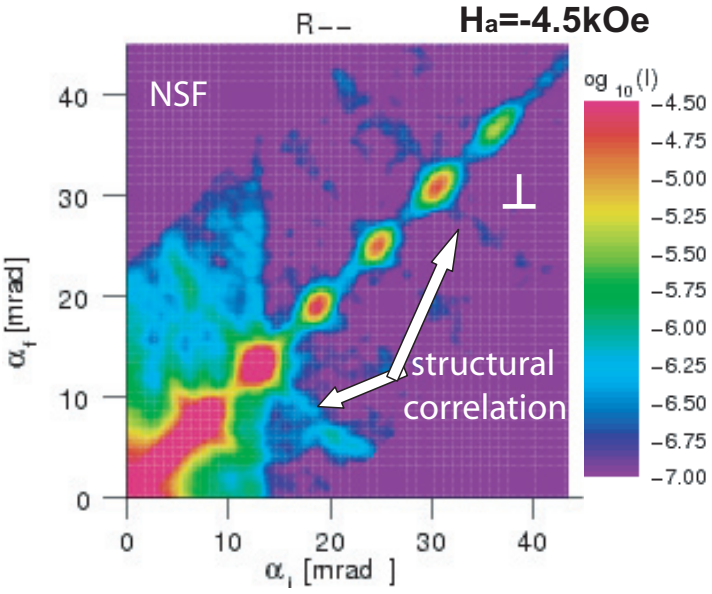

Figure 8. NSF intensity maps from Co/CoO/Au ML measured at −4.5 kOe after perpendicular field cooling.

correlation of these lateral domains is about 200 nm (extending up to one-third of the total thickness). Moreover, these domains remain untrained with field cycling and remain similar during the increasing (figures 7(g) and (h)) and decreasing branches of the hysteresis loop.

One may note that these vertical correlations are clearly different from the domains that we generally observe after parallel field cooling (figure 7(i)). For parallel field cooling, they remain vertically uncorrelated and their lateral correlation extends from 1 to 5 μm at remanence and from 10 to 25 μm at saturation, depending on the strength of the cooling field as has been estimated from our earlier measurements on similar samples [10]. They are typically signified by fluctuations around the mean value of the laterally averaged interaction potential around the reversal point.

Typically the signature of vertical *structural* correlation can be observed in the form of diffuse scattering streaks in the NSF signals (R_{--}) at −4.5 kOe in figure 8. Note that such diffuse scattering streaks across the Bragg peaks are absent in the corresponding SF channel (figure 7(f)), confirming their non-magnetic origin. Our microstructural investigation by XTEM also shows structural vertical correlation of grains. The vertical correlation of structures is seen to be mainly due to the Au (separating layer) and Co layers. Such structural correlation would be present irrespective of the perpendicular cooling or in-plane cooling procedure. Therefore, the domain correlation that we observe for perpendicular cooling alone (and not for in-plane cooling) is independent of its structural correlation.

In the case of collinear coupling—perpendicular to the film plane—one should not expect a considerable exchange bias field along the film plane. Similarly, in the case of collinear coupling—along the film plane—one may not expect vertical correlation of domains. Thus the observed exchange bias field (~ -175 Oe) and the corresponding vertical correlation of domains point to a non-collinear coupling in the system. However, the degree of collinearity could not be directly estimated, as neutron scattering is sensitive to in-plane components alone. Nevertheless, considering an exchange bias field of around −500 Oe along the cooling field

direction (out-of-plane SQUID curve) and its in-plane projection to be around −175 Oe (field variation of PNR data), one can roughly estimate a non-collinearity of around ($\omega =$) 19° away from the film normal.

We believe that competition between two perpendicular anisotropies in the system is responsible for these distinct features:

1. The magnetization reversal mechanism is via predominant coherent rotation (uniform reversal) on both branches of the hysteresis loops (supported by the strong SF signals), i.e. they are symmetric.
2. The magnetic domain structures are vertically and laterally correlated.
3. The domain structures as well as the magnetization reversal mechanism remain almost unchanged with field cycling, i.e. they are microscopically untrained.

These first two contradictory features from our study indicate the co-existence of inhomogeneous magnetic states within the system (sketch in figure 7). The sample forms, in parts, smaller domains (correlated with the neighboring layers and $\leqslant l_{\parallel}$), whereas in other parts, the FM moments (laterally un-correlated and $\geqslant l_{\parallel}$) remain uncorrelated with the neighboring layer.

The average interfacial magnetization vector [32] of a part of the AF grains is coupled to the exchange field of the vertically and laterally uncorrelated portions of the FM. Being perpendicular to the H_{FC} direction, they can create a large torque in the film plane with the applied field, which could obviously rotate the FM magnetization. This alignment of rotatable anisotropy is not disturbed upon field cycling as they are randomly distributed in the film plane. This can thereby lead to the observed untrained behavior.

On the other hand, the average interfacial magnetization vector of the other part of the AF grains is coupled to the exchange field of the portions of the FM magnetization that are vertically and laterally correlated. These portions thus form a non-collinear coupling. The in-plane component of this non-collinear coupling is small and provides the measured exchange field (3.5 times lower than what is observed for conventional field cooling) as we measure along the film plane. The reversal mechanism for these FM moments, as observed, is via the non-uniform mode, which would have also been expected for a conventional in-plane cooling field.

However, the untrained behavior of such small-scale domain structures is interesting as well as surprising. One may recall that in the case of in-plane cooling, the uncorrelated domain structures that are usually visible disappear after the first half of the first field cycle, whereas in the case of out-of-plane field cooling, they remain stable not only after the first half of the first field cycle, but also for the first half of the second field cycle. We compare the diffuse scattering spectra with unpolarized data at room temperature and at remanence . It can be seen from figure 9 that the spectra are typically similar (vertically uncorrelated and $\xi_{\mathrm{RT}} \approx 5.0\,\mu$m) to those after parallel field cooling. This leads to the fact that parallel field cooling has little or no effect on the FM domain structures that exist at RT without any coupling with the AF. Thus, the change in domain characteristics (vertical correlation) can be attributed solely to the out-of-plane unidirectional biasing. Non-collinear coupling mediates the formation of small-scale domains correlated along the thickness of the multilayer stack.

The exchange bias Hamiltonian under perpendicular biasing can be expressed as

$$H_{\mathrm{EB}} \propto J_{\mathrm{E}} \mid S_{\mathrm{AF}} \parallel S_{\mathrm{FM}} \mid \cos\,\eta \propto \sqrt{K_{\mathrm{AF}} A_{\mathrm{AF}}}\,\cos\,\eta. \tag{11}$$

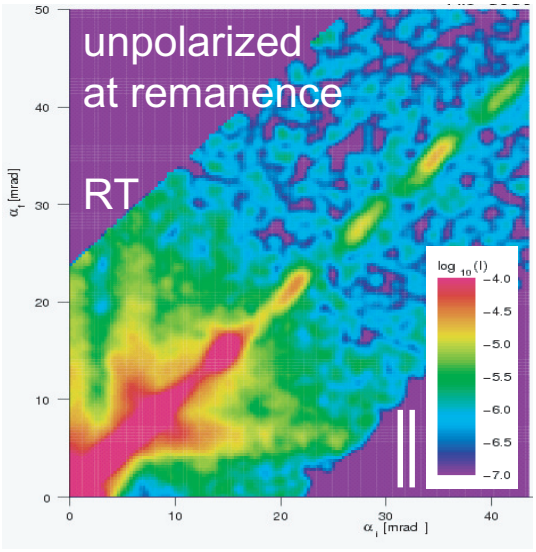

Figure 9. Unpolarized SF intensity map from Co/CoO/Au ML measured at RT and at remanence.

Here S_{FM} and S_{AF} are the AF and FM spins, and A_{AF} is the stiffness [13]. Thus this vertical correlation of domains can be related to AF domains as well, since the dominant factor in the expression for H_{EB} is the AF domain formation. For an AF grain size of $\approx$ 15–20 nm, one may encounter regions of uniform magnetization ($\sim$ domain wall) that have effective anisotropy. A number of grains may contribute to such random anisotropy superimposed on its uniaxial (magnetoelastic) anisotropy.

Training has been a long-standing issue in spin-valve-type magnetic memory devices [33]. It has been shown that in the case of a hard-and-soft layer spin-valve structure, repeated cycling can lead to a decrease in magnetization of the hard layer. Demagnetization results from the formation and motion of domain walls in the soft layer. In exchange biased spin valves, repeated cycling results in the loss of magnetic memory. Thus to achieve stability in device structure, one must get rid of the non-uniform reversal (associated with the so-called asymmetry in magnetization reversal) ensuring reversal via coherent rotation. We have shown that symmetric coherent rotation without any microscopic training can be achieved. This can be realized by inducing an exchange bias by coupling the uncompensated AF moments either with a remanent state of the FM magnetization [10] (in the case of in-plane biased structures) or with the FM moments along a direction perpendicular to the AF axis (in the case of out-of-plane biased structures).

3. Conclusion

In conclusion, we present a novel way of inducing exchange bias in an archetypical AF–FM multilayered system. The uniqueness lies in the fact that the unidirectional anisotropy has been directed perpendicular to the film plane, while the AF anisotropy has been kept along the film plane, resulting in non-collinearity in the coupling. This coupling has brought about some clearly different magnetization behavior for the AF–FM interfacial spins as compared with what is observed for a conventional parallel field cooling case in the same or a similar

system. The magnetization reversal is characterized by symmetric reversal that takes place via non-uniform (vertically correlated domains) and uniform modes and remains untrained with field cycling. Competing perpendicular anisotropic directions, (i) the out-of-plane unidirectional anisotropy and (ii) in-plane AF uniaxial anisotropy, are believed to be responsible for all such features regarding the domain structure correlations (in-plane and out-of-plane) and concomitant magnetization reversal.

Acknowledgments

We would like to thank Ulrike Bloeck for her assistance in the TEM measurements.

Author contributions: AP and SM carried out the neutron measurements, and NP carried out the TEM measurements. AP planned the project, prepared the sample, analyzed the data and wrote the manuscript.

References

[1] Meiklejohn W H and Bean C P 1956 *Phys. Rev.* **102** 1413
[2] Gierlings M, Prandolini M J, Fritzsche H, Gruyters M and Riegel D 2002 *Phys. Rev.* B **65** 092407
[3] Paul A, Kentzinger E, Rücker U and Brückel Th 2006 *Phys. Rev.* B **73** 092410
[4] Paul A, Schneider C M and Stahn J 2007 *Phys. Rev.* B **76** 184424
[5] Nogués J and Schuller I K 1999 *J. Magn. Magn. Mater.* **192** 203
Berkowitz A E and Takano K 1999 *J. Magn. Magn. Mater.* **200** 552
[6] Stiles M D and McMichael R D 1999 *Phys. Rev.* B **59** 3722
[7] Gruyters M *et al* 2008 *Phys. Rev. Lett.* **100** 077205
[8] Fitzsimmons M R, Yashar P, Leighton C, Schuller I K, Nogues J, Majkrzak C F and Dura J A 2000 *Phys. Rev. Lett.* **84** 3986
[9] Radu F, Etzkorn M, Siebrecht R, Schmitte T, Westerholt K and Zabel H 2003 *Phys. Rev.* B **67** 134409
[10] Paul A and Mattauch S 2009 *Appl. Phys. Lett.* **95** 092502
[11] Paul A, Kentzinger E, Rücker U and Brückel Th. 2006 *Phys. Rev.* B **74** 54424
[12] Geshev J, Nicolodi S, Pereira L G, Schmidt J E, Skumryev V, Suriñach S and Baró M D 2008 *Phys. Rev.* B **77** 132407
[13] Nogués J, Moran T J, Lederman D, Schuller I K and Rao K V 1999 *Phys. Rev.* B **59** 6984
Tillmanns A, Oertker S, Beschoten B, Güntherodt G, Eisenmenger J and Schuller I K 2008 *Phys. Rev.* B **78** 012401
[14] Le Graët C, Spenato D, Pogossaian S P, Dekadjvei D T and Youssef J B 2009 *Appl. Phys. Lett.* **94** 262502
[15] Åkerman J, Ström V, Rao K V and Dahlberg E D 2007 *Phys. Rev.* B **76** 144416
[16] Maat S, Takano K, Parkin S S P and Fullerton E 2001 *Phys. Rev. Lett.* B **87** 087202
[17] Ijiri Y, Schulthess T C, Borchers J A, van der Zaag P J and Erwin R W 2007 *Phys. Rev. Lett.* B **99** 147201
[18] Nogués J, Stepanow S, Bollero A, Sort J, Dieny B, Nolting F and Gambardella P 2009 *Appl. Phys. Lett.* **95** 152515
[19] Wang J, Kuch W, Chelaru L I, Offi F and Kotsugi M 2005 *Appl. Phys. Lett.* **86** 122504
[20] Shipton E, Chan K, Hauet T, Hellwig O and Fullerton E E 2009 *Appl. Phys. Lett.* **95** 132509
[21] Zhou S M, Yuana S J and Sun L 2005 *J. Magn. Magn. Mater.* **285** 211
[22] Garcia F, Casali G, Auffret S, Rodmacq B and Dieny B 2002 *J. Appl. Phys.* **91** 6905
[23] Gruyters M 2007 *Europhys. Lett.* **77** 57006
[24] Barnier Y, Pauthenet R and Rimet G 1961 *C. R. Acad. Sci. Paris* **252** 2839
[25] Toperverg B P 2002 Polarized neutron scattering *Matter and Materials* vol 12 ed Th Brückel and W Schweika (Jülich: Forschungszentrum Jülich GmbH, Institut für Festkörperforschung) p 274

[26] Lee W-T, te Velthuis S G E, Felcher G P, Klose F, Gredig T and Dahlberg E D 2002 *Phys. Rev.* B **65** 224417
[27] Theis-Bröhl K *et al* 2008 *New J. Phys.* **10** 093021
[28] Zabel H *et al* 2007 *Handbook of Magnetism and Advanced Magnetic Materials* ed H Kronmuller and S Parkin (New York: Wiley) p 1237
[29] Majkrzak C F and Berk N F 1996 *Physica* B **221** 520
[30] Paul A, Bürgler D, Luysberg M and Grünberg P 2004 *Europhys. Lett.* **68** 233
[31] Hautot D, Pankhurst Q A and Dobson J 2005 *Rev. Sci. Instrum.* **76** 045101
[32] Gredig T, Krivotov I N, Merton C, Goldman A M and Dahlberg E D 2000 *J. Appl. Phys.* **87** 6418
[33] Gider S, Runge B-U, Marley A C and Parkin S S P 1998 *Science* **281** 797